5-22

SANDIA REPORT

SAND96–0883 • UC–401
Unlimited Release
Printed April 1996

Simplified Models of Growth, Defect Formation, and Thermal Conductivity in Diamond Chemical Vapor Deposition

Michael E. Coltrin, David S. Dandy

Prepared by
Sandia National Laboratories
Albuquerque, New Mexico 87185 and Livermore, California 94550
for the United States Department of Energy
under Contract DE-AC04-94AL85000

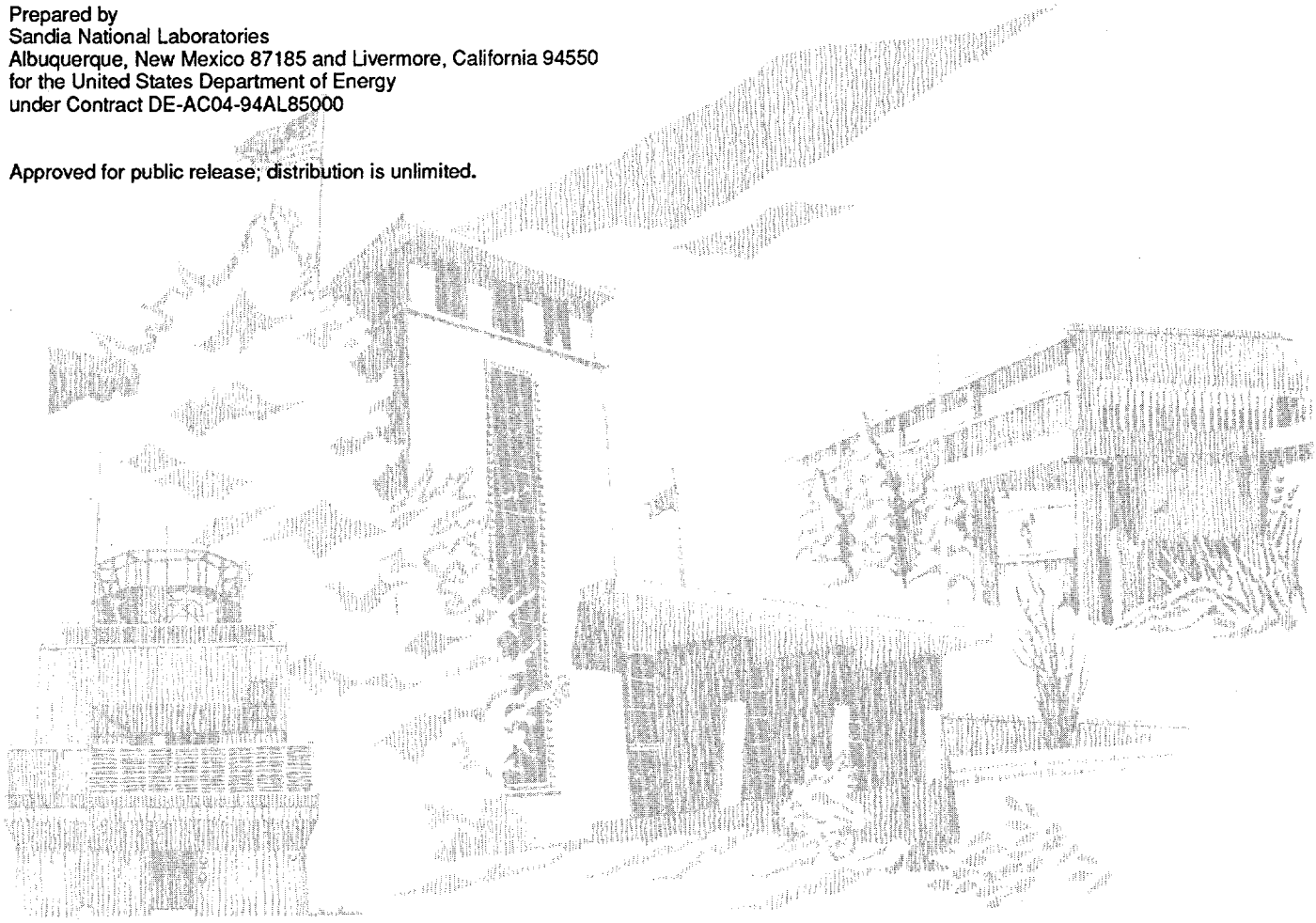

Issued by Sandia National Laboratories, operated for the United States Department of Energy by Sandia Corporation.

Available to DOE and DOE contractors from
Office of Scientific and Technical Information
PO Box 62
Oak Ridge, TN 37831

Prices available from (615) 576-8401, FTS 626-8401

Available to the public from
National Technical Information Service
US Department of Commerce
5285 Port Royal Rd
Springfield, VA 22161

NTIS price codes
Printed copy: A03
Microfiche copy: A01

SAND96-0883
Unlimited Release
Printed April 1996

Distribution
Category UC-401

SIMPLIFIED MODELS OF GROWTH, DEFECT FORMATION, AND THERMAL CONDUCTIVITY IN DIAMOND CHEMICAL VAPOR DEPOSITION

MICHAEL E. COLTRIN
Chemical Processing Sciences Dept.
Sandia National Laboratories
Albuquerque, New Mexico 87185

DAVID S. DANDY
Dept. of Chemical Engineering
Colorado State University
Fort Collins, Colorado 80523

ABSTRACT

This report presents a simplified surface reaction mechanism for the Chemical Vapor Deposition (CVD) of diamond thin films. The mechanism also accounts for formation of point defects in the diamond lattice, an alternate, undesirable reaction pathway. Both methyl radicals and atomic carbon are considered as growth precursors. While not rigorous in all its mechanistic details, the mechanism is useful in describing the CVD diamond process over a wide range of reaction conditions. It should find utility in reactor modeling studies, for example in optimizing diamond growth rate while minimizing defect formation. This report also presents a simple model relating the diamond point-defect density to the thermal conductivity of the material.

Introduction

Much theoretical analysis has been done on the elementary heterogeneous chemical reactions leading to diamond deposition. There will likely never be full agreement on the details of the process. However, it has been found that relatively few reactions are needed if the goal is limited to an accurate description of deposition rates. The goal in this work is to develop the simplest possible reaction mechanism to be used in our reactor models which still captures the features of interest. This report describes a simplified surface reaction mechanism for the growth of diamond and the formation of point defects in the material. The reaction scheme is not intended to be mechanistically correct in all its details. However, it should be adequate to describe the competition between these two growth paths and how that competition changes with reactor conditions. It will thus be useful in reactor-scaling studies.

A fundamental limitation in commercializing the diamond CVD process has been the inability to grow diamond of "high quality" while maintaining high deposition rates. For example, high deposition rates are readily achieved by increasing methane feedgas flow rates, but this is accompanied by a decrease in diamond quality. Although there are a number of potential measures that could be used as a metric for diamond quality, this work focuses on the diamond's thermal conductivity (a key property in its application for thermal management). This work presents a simple model connecting the density of point defects (as calculated with the simple reaction mechanism mentioned above) to the material's thermal conductivity. The relationship described is simple enough to be used in reactor scaling exercises to optimize growth rate and thermal conductivity.

Simplified Reaction Mechanism

Our earlier modeling work [1] showed that CH_3, atomic-C, or a combination of the two could be responsible for bringing carbon to the surface in dc arc jet systems, depending on reaction conditions. It has also been observed that, depending upon growth conditions, point defects are incorporated into the lattice.

Goodwin has given a simplified set of surface reactions that can describe diamond growth rates over a wide range of conditions [2]. The reactions in his simplified mechanism are listed as numbers S1 through S6 in Table I. The four surface species listed in Table I are: CH(s), a surface carbon bonded to a hydrogen; C*(s), a surface carbon with one dangling bond, i.e., a radical site; CM(s), a CH_3 bonded to a surface carbon atom; and CM*(s), a CH_2 group bonded to a surface carbon, which is also has one dangling bond. Two bulk species are included in Table I, a diamond lattice atom D, and a lattice point defect P_d. A simplified set of reactions, such as listed in Table I, is not intended to be mechanistically correct in its detail, but just to capture the main features of the CVD process. Describing the process through such a sequence of "generic" steps also allows one to estimate reasonable rate constants for use in a kinetic simulation.

Goodwin provides rate constants for reactions S1–S5 (at 1200 K), which were set to match rates from a variety of H-recombination experiments, molecular dynamics simulations, an empirical fit to deposition rates predicted by the more detailed deposition mechanism of Harris [3], and to give an average lifetime of 100 μs for surface CH_3 [2]. (The rate constant for reaction S6 was not given explicitly by Goodwin, but was listed as "fast." At steady state, the deposition rate is independent of this rate constant, and a value sufficiently "fast" was supplied for the simulations.) As in the mechanism presented by Goodwin, activation energies are not supplied for this simplified heterogeneous kinetics model—it is

intended to be valid within some small range of 1200 K. The model was tested with 7300 cal/mole activation energies for the H-abstraction reactions (S1, S5, S6) [4], and with the CH_3 desorption (S4) activation energy set to our earlier estimate of the bond strength [1]. With activation energies present the model was in quantitative agreement with experiment regarding the existence of a maximum growth rate with T_s ($\approx$ 1150 K) [5-7]. However, the model did not correctly capture the observed 20 kcal/mole effective activation energy for growth for T_s < 1150 K [6,7]; the predicted activation energy was approximately 10 kcal/mole too low.

Reaction S7 was included to account for deposition from C-atoms. Earlier modeling studies of the dc arc-jet deposition system show that under certain conditions (high H_2-dissociation fractions) C was the most abundant carbon-containing species in the gas [1,8]. Because C is a very reactive species, its contribution to the diamond deposition should not be neglected. The rate constant for S7 was set equal to that of reaction S3. Goodwin has pointed out [2] that reactions S1 through S6 do a good job of reproducing measured growth rates over a wide range of conditions. For conditions typical of the dc arc-jet reactor, Figure 1 shows that the diamond growth rate scales linearly with CH_3 mole fraction at the surface using the set of reactions in Table I.

Under conditions of high growth rate, defects can be incorporated into the diamond lattice. Such defects could be sp^2 in nature, formed via a β-bond cleavage from unimolecular decomposition of adjacent C*(s) and CH(s) species; Butler and Woodin [9] present a simple kinetic analysis for growth of this type of defect. They also discuss sp^3 defects, characterized by hydrogen bonded to sp^3 carbons, in which subsequent layers of carbon add to the surface before all of the surface hydrogen atoms have been displaced through H-abstraction and C-C bond formation reactions [9]. However, no specific kinetic scheme was suggested for formation of these defects.

Reactions S8 and S9 have been included in our reduced surface reaction mechanism in Table I to describe "over-growth" of an sp^3 defect, trapping hydrogen into the lattice. Although not to be considered elementary reactions, S8 and S9 should nonetheless capture the important features. These reactions involve a reactive carbon species (either CH_3 or C) reacting with the CM*(s) species, as a competition to the diamond growth reaction of CM*(s), reaction S6. Thus, reactions S8 and S9 will be important under conditions of high growth rate when the concentration of carbon species becomes larger relative to gas-phase H.

A few comments about the form of reactions S8 and S9 are in order. First, Butler and Woodin [9] include a reaction similar to S8 (except forming a surface C_2H_5 species) as part of a proposed mechanism for normal diamond growth on the (110) surface. Thus, a reminder that the reactions in Table I have to be considered generic rather than elementary. Second, note that S8 and S9 are first-order in the surface reactant CM*(s). Comments will made later about the scaling of lattice-defect formation rates with respect to the reaction order of their creation. Finally, rate constant information is not available for reactions S8 and S9. The value given in Table I was set to yield defect densities in the parts-per-million range, consistent with EPR measurements [10]. For purposes of the next discussion, the set of reactions S1–S9 will be referred to as M1 (mechanism 1).

Goodwin [2] also included arguments concerning the scaling of defect formation with process conditions. The basic assumption in that work was that defects were formed by reaction of a surface adsorbate with a nearby adsorbate before it had been fully incorporated

into the lattice. However, a precise chemical reaction for forming the defect was not mentioned. This simple picture is similar in spirit to the Butler and Woodin [9] picture of sp^3 defect formation just mentioned. The assumption that the defect formation reaction was second-order in surface reactants leads to a simple scaling relationship [2] between defect fraction X_d, growth rate G, and hydrogen-atom molar concentration [H]:

$$X_d \propto \frac{G}{[\mathrm{H}]^2}. \tag{1}$$

Goodwin was careful to point out the exact form of the scaling of defect formation is uncertain, and that equation (1) would more generally be written with an exponent n in the denominator, where n is determined experimentally.

Note that the scaling of defect fraction depends upon the order of the surface reaction that forms the defect. This is illustrated by comparing the scaling of reaction set M1 with predictions using a defect-formation reaction second order in the surface adsorbate, such as

$$2\ \mathrm{CM(s)} \rightarrow \mathrm{CM(s)} + \mathrm{CH(s)} + \mathrm{H_2} + \mathrm{P_d}. \tag{S10}$$

The precise form of such a second order reaction, especially the list of products, is uncertain. However, reaction S10 will suffice for the purpose of examining the dependence of defect formation scaling with respect to the order of the surface reaction. For this example, the rate constant for S10 was set to 3.0×10^8; this value was chosen to give roughly the same defect formation rates as reaction set M1 for a nominal arc-jet condition with H-atom mole fraction at the surface of 0.02 and CH_3 mole fraction at the surface of 0.001. The set of reactions S1–S7 and S10 will be denoted M2.

Figure 2 shows that, for a fixed concentration of H at the surface, the lattice defect fraction increases linearly with CH_3 concentration at the surface for both sets of reactions M1 and M2. (Here the defect fraction is taken to be the ratio of the defect growth rate to the diamond growth rate.) The defect fraction will also scale linearly with C-atom concentration at the surface for set M1, but for simplicity of discussion is not plotted. Since growth rate and defect fraction both increase linearly with CH_3 fraction, it is immediately clear that defect fraction will increase (and diamond "quality" will decrease) as growth rate increases for either set of reactions.

The diamond growth rate attainable for a fixed defect density scales differently for the two sets of reactions M1 and M2, as illustrated in Figure 3. For this plot, defect density was specified to be 10^{-6} mole fraction, and for each value of [H], the amount of CH_3 necessary to attain that defect fraction was determined; the allowable CH_3 mole fraction at fixed defect density as a function of [H] is shown in Figure 4. For larger values of [H], Figure 3 shows that set M1 predicts the growth rate at fixed defect density will scale approximately linearly with H concentration. For reaction set M2, the attainable growth rate at fixed defect density scales quadratically with [H]; this is consistent with the formula given by Goodwin [2], equation (1). For the defect mechanism that includes the first-order (in surface adsorbate) reactions, set M1, the allowable CH_3 increases linearly with H concentration (solid curve in Figure 4). For reaction set M2, which includes the second-order defect formation reaction S10, the allowable CH_3 increases quadratically with H (dashed curve in Figure 4).

The difference in scaling of growth rate with H-atoms at constant defect density has implications to making higher powered arc-jet reactors. If defect formation scales as in the first-order reaction set M1, then increasing the arc-jet power would increase H-atom production, giving approximately a linearly increase in attainable growth rate. However, if the defect formation is second order in surface adsorbates as in set M2, growth rate at constant quality increases quadratically with [H], indicating much larger pay-off in going to higher power (higher H_2 dissociation fraction).

Relating Thermal Conductivity and Defect Density

It is clearly desirable to grow diamond with a minimum of defects. However, the property of interest to the consumer for the diamond film is likely to be some other measure of quality, such as thermal conductivity. As mentioned earlier, there is a typically a trade-off between diamond growth rate and film thermal conductivity, illustrated in Figure 5. This section presents a simple formula to relate concentration of lattice point defects to the material's thermal conductivity in an attempt to explain this limitation. The discussion begins with some general comments about thermal conductivity.

The thermal conductivity of a gas can be obtained from the kinetic theory of gases as

$$\lambda = \frac{1}{3} C v l, \tag{2}$$

where v is the particle's average velocity, l is the mean free path, and C is the heat capacity. For a crystal, equation (2) is generalized as

$$\lambda = \frac{1}{3} \sum_{\alpha} C_{\alpha} v_{\alpha} l_{\alpha}, \tag{3}$$

where α denotes the excitation mechanism, i.e., particles or waves [11]. The carriers of heat are typically lattice waves and free electrons (in the case of metals or semi-conductors). The mean free path of these carriers is limited by a number of different scattering processes, such as scattering by other lattice waves, defects, or grain boundaries in the crystal [11]. The various scattering processes all contribute to the mean free path as [12]

$$\frac{1}{l(\omega)} = \sum_{i} \frac{1}{l_i(\omega)}. \tag{4}$$

The form of equation (4) indicates that the mean free path has a phonon frequency ω dependence, which can differ between the various scattering mechanisms.

The approximation will be made that the thermal conductivity is proportional to the mean free path l,

$$\lambda \propto l \tag{5}$$

as in Eqs. (2) and (3), and that this mean free path has two components: (1) l_D due to point-defects in the lattice, and (2) an intrinsic component l_I due to all other scattering processes in the diamond lattice. By analogy with Eq (4), the two are combined as

$$\frac{1}{l} = \frac{1}{l_I} + \frac{1}{l_D}. \tag{6}$$

Thus,

$$\lambda = \frac{c l_I l_D}{l_I + l_D}. \tag{7}$$

The mean free path l_D due to point-defects is assumed to be related to the defect density as

$$l_D = \rho_D^{-1/3}. \tag{8}$$

Equation (7) is a simple relationship requiring two empirical constants, i.e., c the proportionality constant, and l_I . Newton, Cox and Baker [10] have used EPR to measure defect density in a series of diamond samples for which the thermal conductivities were also known. This data set provides the calibration of the simple formula in equation (7). The constants obtained by fitting to the data points at 0,31 and 2.78 ppm defect density are $l_I = 4.274 \times 10^{-6}$ cm and $c = 9.203 \times 10^{6}$ W/cm^2/K. A comparison between the measured data and the simple fit of equation (7) is shown in Figure 6.

The growth and defect-formation mechanism of Table I was used to predict diamond growth rate and defect density as a function of H and CH_3 mole fraction (at the surface), then equation (7) was used to convert defect density to thermal conductivity. The resulting predictions shown in Figure 7 exhibit the qualitative features seen experimentally in Figure 5. That is: (a) thermal conductivity drops off with increasing growth rate; (b) increasing H-atom concentration (with CH_3 held fixed) yields higher growth rates and higher thermal conductivity; and (c) increasing CH_3 (with H held fixed) increases growth rate but decreases the thermal conductivity.

IBIS Associates has been studying the economics of various CVD diamond growth approaches. Their models incorporate scaling relationships for transport and kinetic processes in CVD diamond reactors, primarily based on the work of Goodwin [2]. The models predict physical quantities such as deposition rate, reagent usage, etc. The IBIS models then estimate the cost of running the process, and ultimately the cost of the diamond films produced.

The simplified models for defect formation and the relationship to thermal conductivity have also been incorporated into the IBIS models. The defect and thermal conductivity models add a valuable dimension to the economic models by pointing out that the cost of the diamond product depends strongly upon the quality of the diamond that is required. Figure 8 illustrates one such analysis done for combustion synthesis of diamond films. Because of the trade-off between growth rate and quality, if an application requires very high thermal conductivity it comes at the expense of low growth rate, and thus higher cost. However, for applications requiring lower thermal conductivity (say 5 W/cm/K) the cost of the diamond will be much less.

Acknowledgments

The authors thank David Goodwin and Richard Woodin for helpful discussions regarding development and testing of the work discussed here. We also thank Adam Singer of IBIS Associates for providing the cost modeling information.

References

1 M. E. Coltrin and D. S. Dandy, J. Appl. Phys. **74**, 5803 (1993).
2 D. G. Goodwin, J. Appl. Phys. **74**, 6888 (1993).
3 S. J. Harris, Appl. Phys. Lett. **56**, 2298 (1990).
4 C. K. Westbrook, J. Warnatz, and W. J. Pitz, Proceedings of *Twenty-second Symposium (International) on Combustion* (Seattle, Washington, 1988), p. 893.
5 E. Kondoh, T. Ohta, T. Mitomo, and K. Ohtsuka, Appl. Phys. Lett. **59**, 488 (1991).
6 E. Kondoh, T. Ohta, T. Mitomo, and K. Ohtsuka, J. Appl. Phys. **73**, 3041 (1993).
7 S. J. Harris and A. M. Weiner, J. Appl. Phys. **75**, 5026 (1994).
8 B. W. Yu and S. L. Girshick, J. Appl. Phys. **75**, 3914 (1994).
9 J. E. Butler and R. L. Woodin, Phil. Trans. Royal Soc. **342**, 209 (1993).
10 M. E. Newton, A. Cox, and J. M. Baker, personal communication (1994).
11 P. G. Klemens in "*Thermal Conductivity,*" vol. I, R. P. Tye, ed., (Academic Press, London, 1969), p. 2-3.
12 *ibid*, p. 17.
13 A. Singer, IBIS Associates, private communication.

Table I. Surface reaction mechanism describing the growth of diamond, D, and the formation of buried point defects, P_d, from C and CH_3 precursors.

Number	Reaction	k_i*
S1	$CH(s) + H \rightarrow C^*(s) + H_2$	2.9×10^{12}
S2	$C^*(s) + H \rightarrow CH(s)$	1.7×10^{13}
S3	$C^*(s) + CH_3 \rightarrow CM(s)$	3.3×10^{12}
S4	$CM(s) \rightarrow C^*(s) + CH_3$	1.0×10^{4}
S5	$CM(s) + H \rightarrow CM^*(s) + H_2$	2.0×10^{12}
S6	$CM^*(s) + H \rightarrow CH(s) + H_2 + D$	4.0×10^{13}
S7	$C^*(s) + C \rightarrow C^*(s) + D$	3.3×10^{12}
S8	$CM^*(s) + CH_3 \rightarrow CM(s) + P_d + H_2$	7.5×10^{8}
S9	$CM^*(s) + C \rightarrow C^*(s) + P_d + D + H_2$	7.5×10^{8}

* (k_i in moles, cubic centimeters, and seconds; valid at 1200 K.)

FIGURE CAPTIONS

Figure 1: Diamond growth rate as a function of CH_3 mole fraction using the mechanism from Table I. Other conditions for the calculation: H mole fraction = 0.02, with the remainder of the gas H_2, 20 Torr total pressure, surface temperature 1200 K.

Figure 2: Calculated defect mole fraction as a function of CH_3 mole fraction using reaction sets M1 (solid line) and M2 (dashed line). See text for definition of reaction sets. Other conditions are the same as in Figure 1.

Figure 3: Growth rate as a function of H mole fraction obtained for a fixed defect mole fraction of 10^{-6} using reaction sets M1 (solid line) and M2 (dashed line). The CH_3 concentration was adjusted to obtain the desired defect fraction (see Figure 2). Other conditions are the same as in Figure 1.

Figure 4: CH_3 mole fraction needed to obtain a growth rate at constant defect density of 10^{-6} as a function of gas-phase H mole fraction. Other conditions are the same as in Figure 1.

Figure 5: Thermal conductivity of diamond films plotted as a function of the growth rate for that sample. Families of curves are for increasing arc-jet powers, and thus increasing H-atom fraction at the deposition surface. (Data from Norton Company, with the actual values of the growth rates removed to protect proprietary information.)

Figure 6: Thermal conductivity of diamond samples plotted against the measured defect density determined by EPR [10]. The diamond symbols mark the experimental results; triangles are calculated from the simplified thermal conductivity model of equation (7).

Figure 7: Calculated thermal conductivity as a function of growth rate using reaction set M1 and equation (7). H-atom mole fraction is held fixed along each of the three curves, while CH_3 mole fraction is increased. The dashed lines denote constant values of CH_3. Calculations are for 20 Torr total pressure, with H and CH_3 mole fractions typical of a hot-filament environment.

Figure 8: Predicted cost of diamond film as a function of the required thermal conductivity from the IBIS cost models [13]. (This plot is meant to be illustrative only. Many assumptions in the economic models can change the predicted costs dramatically.)

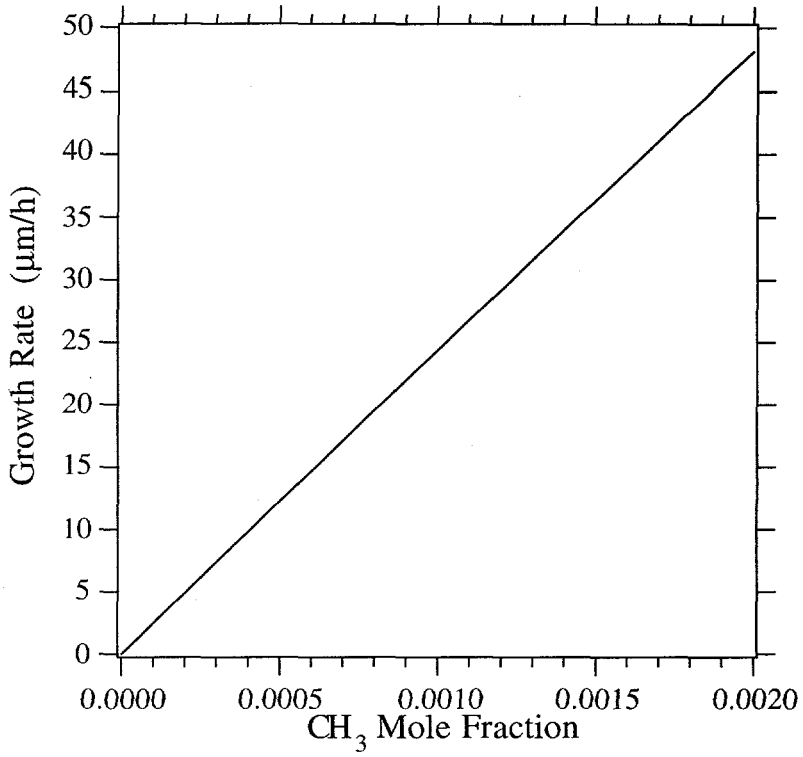

Figure 1.

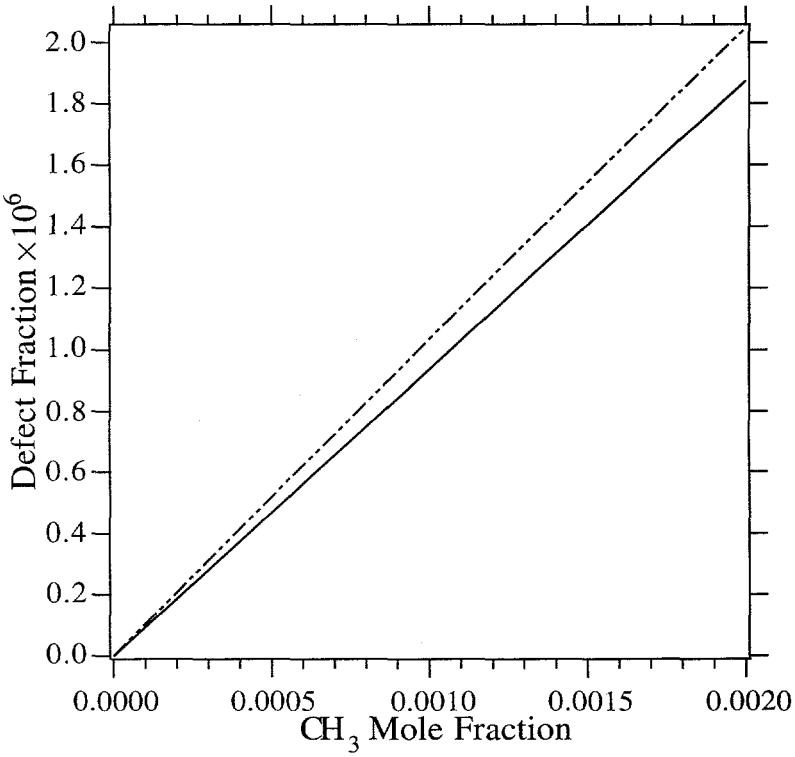

Figure 2.

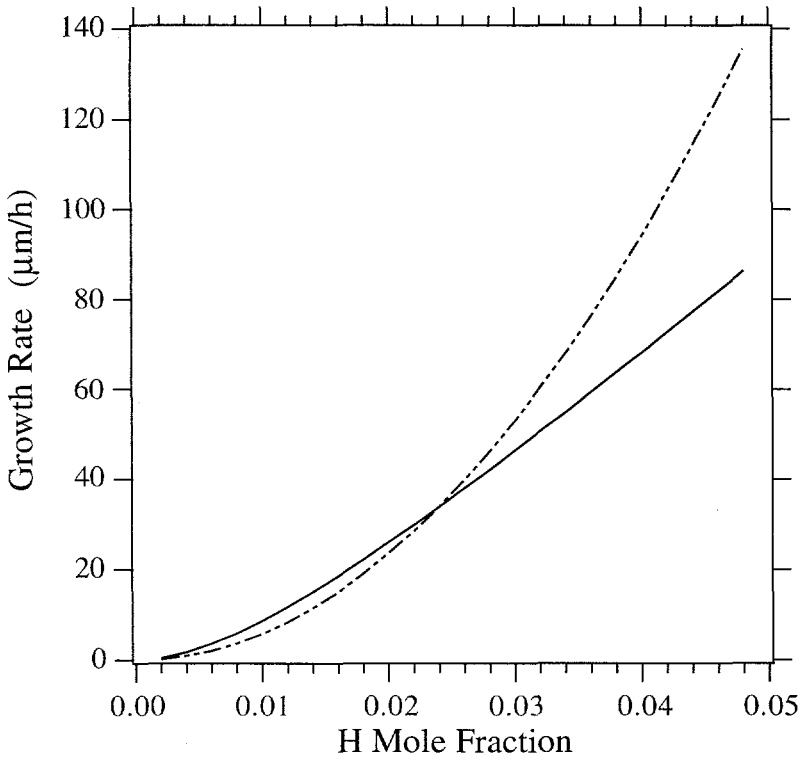

Figure 3.

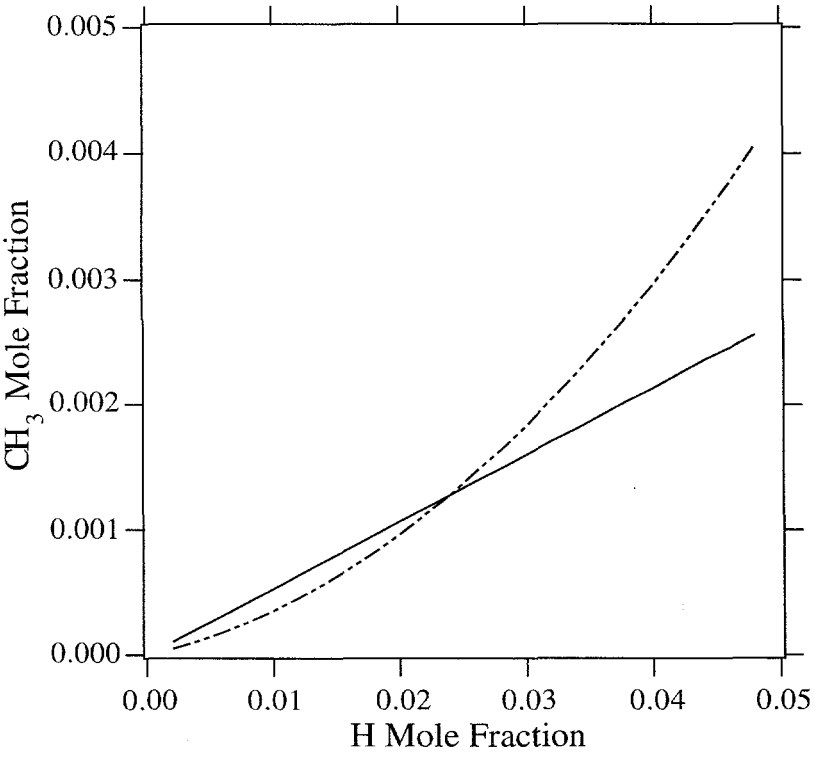

Figure 4.

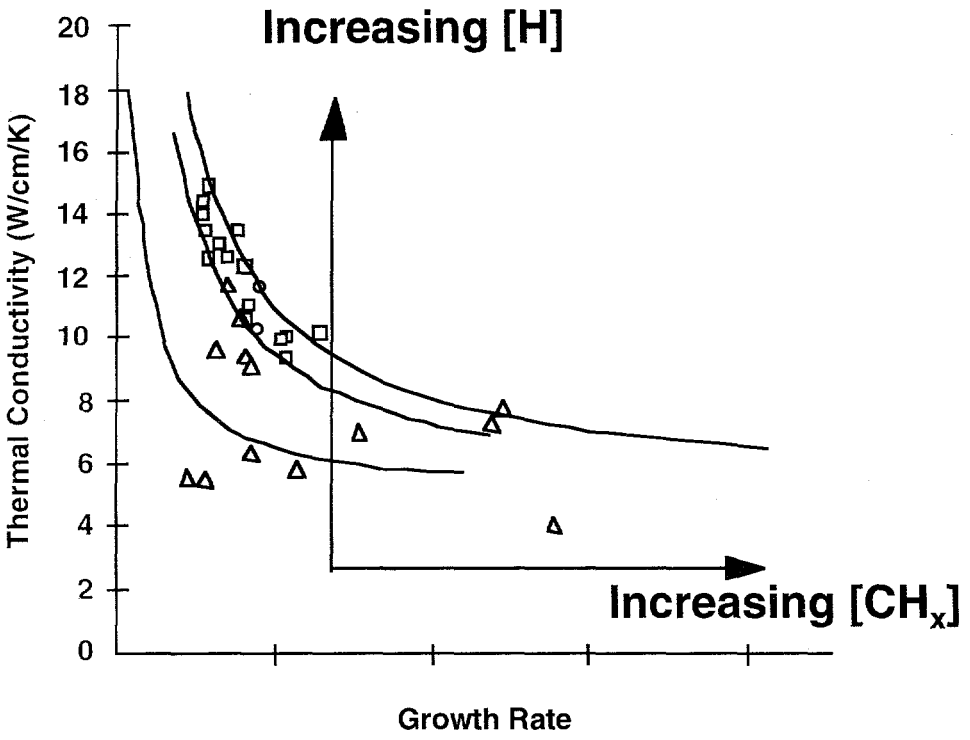

Figure 5.

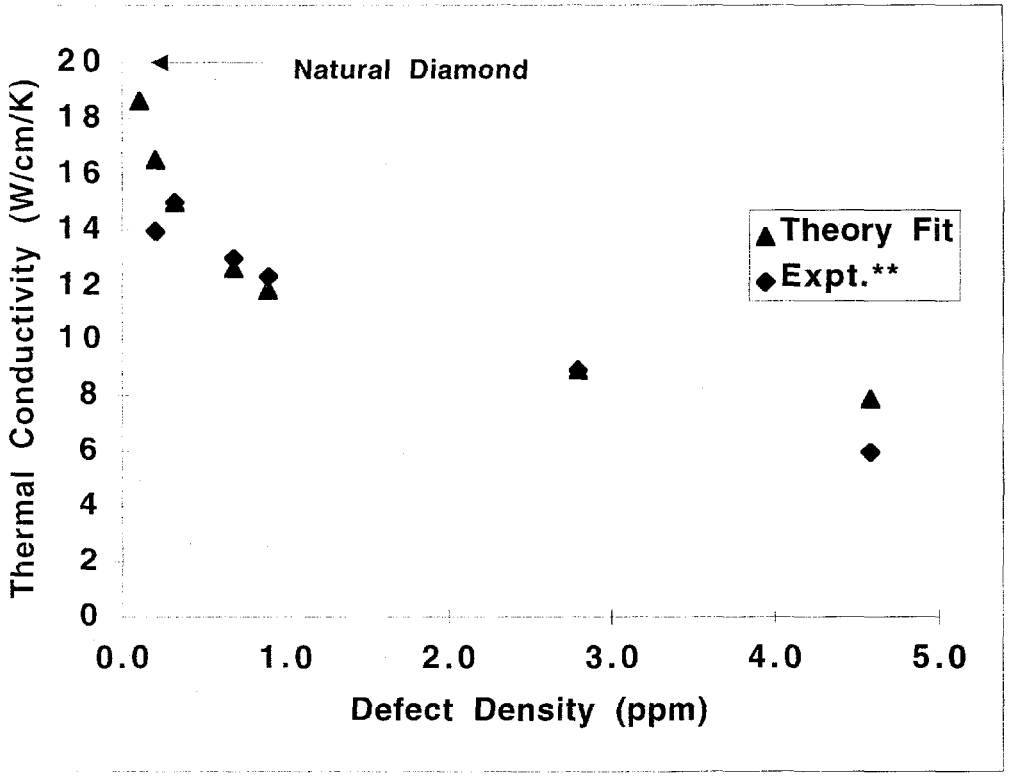

Figure 6.

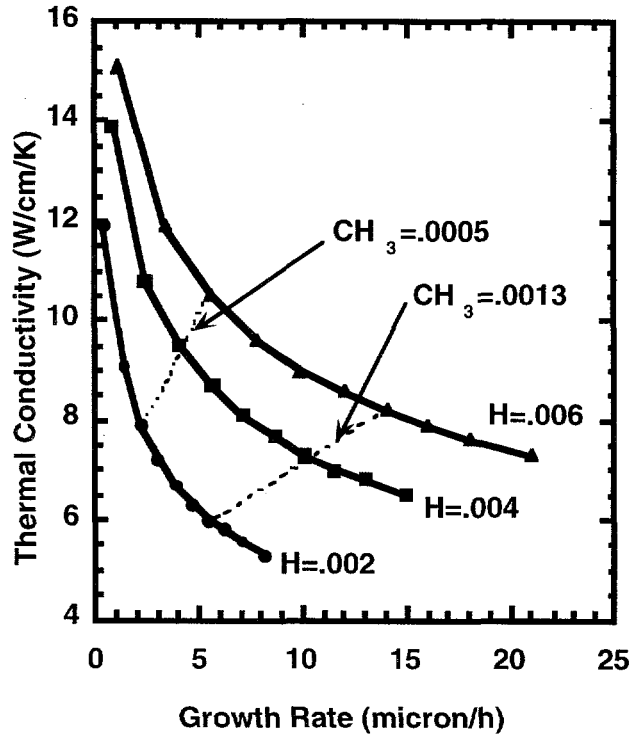

Figure 7.

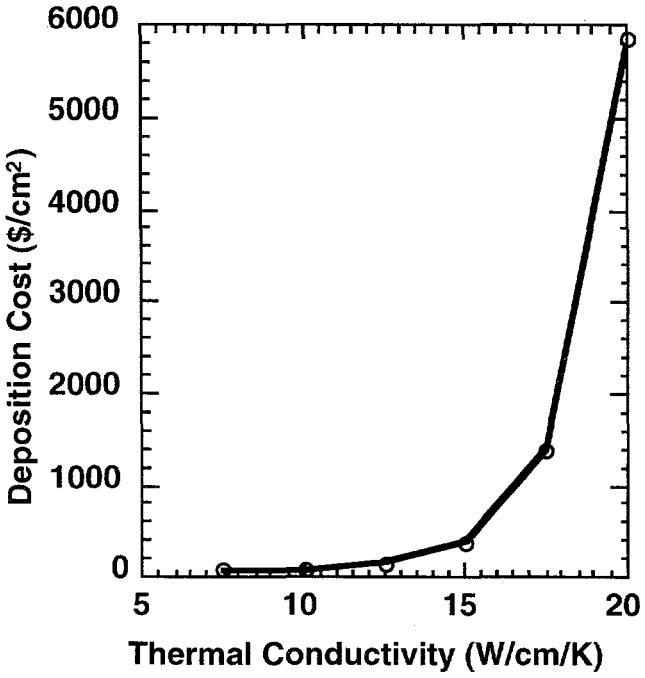

Figure 8.

INITIAL DISTRIBUTION
UNLIMITED RELEASE

John Angus
Department of Chemical Engineering
Case Western Reserve University
10900 Euclid Avenue
Cleveland, OH 44106-7217

Tom Badgwell
Department of Chemical Engineering
Rice University
P.O. Box 1892
Houston, TX 77251

William Barker
8514 Oakford Drive
Springfield, VA 22152

Kim Bigelow
Norton Company
Goddard Road
Northboro, MA 01532-1545

John V. Busch
IBIS Associates, Inc.
55 William Street, Suite 220
Wellesley, MA 02181

James E. Butler
Naval Research Laboratory
Chemistry Division, Code 6174
Washington, D.C. 20375-5000

Mark A. Cappelli
Mechanical Engineering Department
High Temperature Gas Dynamics Laboratory, Building 520
Stanford University
Stanford, CA 94305-3032

David S. Dandy
Department of Chemical Engineering
Colorado State University
Ft. Collins, CO 80523

Michael Frenklach
Department of Mechanical Engineering
University of California at Berkeley
Berkeley, CA 94720-1740

David G. Goodwin
Division of Engineering and Applied Sciences 104-44
California Institute of Technology

Pasadena, CA 91125

Steven J. Harris
Physical Chemistry Department
General Motors Research Laboratories
Warren, MI 48090-9055

Steve Jaffe
Norton Company
14 Mason
Irvine, CA 92718

Jay Jeffries
Molecular Physics Laboratory
SRI International
Menlo Park, CA 94025

Klavs F. Jensen
Department of Chemical Engineering
Massachusetts Institute of Technology
Cambridge, MA 02139

Adam Singer
IBIS Associates, Inc.
55 William Street, Suite 220
Wellesley, MA 02181

Henry Windischmann
Norton Company
Goddard Road
Northboro, MA 01532-1545

Richard L. Woodin
Crystalline Materials Corporation
2311A Old Crow Canyon Road
San Ramon, CA 94583

0367 R. J. Buss, 1812
0601 J. Y. Tsao, 1126
0601 M. E. Bartram, 1126
0601 W. G. Breiland, 1126
0601 M. E. Coltrin, 1126 (50)
0601 J. R. Creighton, 1126
0601 P. Ho, 1126
0601 H. K. Moffat, 1126 (10)
0827 J. Johannes, 9114
1427 P. L. Mattern, 1100
Attn: S. T. Picraux, 1112
J. Nelson, 1113
T. A. Michalske, 1114
G. A. Samara, 1152
E. B. Stechel, 1153
9042 C. M. Hartwig, 8345
9042 R. J. Kee, 8303

9042 E. Meeks, 8345
9043 P. E. Nielan, 8342
9052 M. D. Allendorf, 8361
9214 C. F. Melius, 8117
9018 Central Technical Files, 8523-2
8099 Technical Library, 414 (5)
0619 Document Processing, 7613-2 (2)
For DOE/OSTI

DISCLAIMER